
Volume 71, issues 1–2
May 2008
ISSN 0924-7963
ELSEVIER
JOURNAL OF
MARINE
SYSTEMS

Available online at www.sciencedirect.com
ScienceDirect
Journal of Marine Systems 71 (2008) 131–148
JOURNAL OF MARINE SYSTEMS
www.elsevier.com/locate/jmarsys

Wave-current interaction in coastal waters: Effects on the bottom-shear stress

P. Rosales [a,b,*], F.J. Ocampo-Torres [b], P. Osuna [b], J. Monbaliu [c], R. Padilla-Hernández [d]

[a] *Instituto Tecnológico de Guaymas, Carretera al Varadero Nacional km. 4, Guaymas, Sonora, Mexico*
[b] *Centro de Investigación Científica y de Educación Superior de Ensenada, Km 107 Carretera Tijuana-Ensenada, Ensenada, B.C., 22860, Mexico*
[c] *Hydraulics Laboratory, Katholieke Universiteit Leuven, Kasteelpark Arenberg 40, 3001 Heverlee, Belgium*
[d] *Universidad Autónoma de Tamaulipas, Tampico-Madero, Tamaulipas, Mexico*

Received 6 October 2005; received in revised form 4 June 2007; accepted 20 June 2007
Available online 13 July 2007

Abstract

Computer simulations of wave and current fields in the southern North Sea were made with a coupled-models system to study the influence of wave–current interactions on the bottom-shear stress in coastal waters. A third-generation wave-spectral model is coupled with a tide-surge model, which provides current and water level information to take into account wave–current interactions, to calculate the bottom stress. Two different expressions for bottom friction are used; one derived from the JONSWAP experiment, and a second given by Christoffersen and Jonsson that takes into account wave–current interaction at the bottom. The coupled-models system is applied to four nested grids to achieve fine spatial resolution near the Belgium coast. Two events of moderate to high waves are analyzed. Those two events are associated with different wind regimes; SW winds for the first period and NW for the second. The calculations of bottom-shear stress when taking into account wave–current interactions are compared with reference runs where only waves are considered to calculate the energy dissipation at the bottom. Small differences in the bottom-shear stress results are observed mainly related to the water-level variation caused by tides, when coupled and uncoupled runs using the JONSWAP expression were compared. However, when wave–current interactions are taken into account using the expression of Christoffersen and Jonsson, the calculated maximum bottom stress is usually doubled for coupled-model runs compared to the reference runs. The results clearly show that the formulation of the bottom-friction dissipation that accounts for the effect of wave–current interaction has quite a significant effect on the determination of the bottom-shear stress.

Keywords: Bottom friction; Waves; Currents; Coupling numerical models

1. Introduction

When waves enter shallow waters their interactions with other processes are intensified (e.g. tides and surge). Such interactions modify the environment and hence the wave properties. The response of waves to the interaction with an inhomogeneous current field has been described by Jonsson (1990). In the complex conditions of coastal waters, waves are involved in interactions with wind, bottom processes, and ambient currents, whose dynamics are dominated by wave-bottom boundary-layer processes. Such interactions enhance turbulence within the bottom boundary layer, increasing energy dissipation

* Corresponding author. Instituto Tecnológico de Guaymas, Carretera al Varadero Nacional km. 4, Guaymas, Sonora, Mexico. Fax: +52 646 175 0574x24000.
E-mail address: prosales@cicese.mx (P. Rosales).

0924-7963/$ - see front matter
doi:10.1016/j.jmarsys.2007.06.006

of waves and tides. Understanding the wave–current bottom-interaction processes is of great relevance to determine coupling strength and quantify bottom-shear stresses, which would allow us to compute energy loss by waves and tides. A proper evaluation of sediment transport would eventually follow.

In coastal environments, the superposition of flows associated with waves and currents results in the overlapping of bottom boundary layers of different scales, i.e. a wave bottom-boundary layer embedded in the current bottom-boundary layer. High turbulence intensity within the thin wave bottom-boundary layer causes the current to experience a higher bottom resistance in the presence of waves, in comparison to when waves are absent. Conversely, the wave bottom-boundary-layer flow will also be affected by the presence of currents.

A number of models to describe bottom-friction dissipation have been proposed. They can be classified into time-invariant eddy-viscosity models and mixing-length models (Malarkey and Davies, 1998). The most representative of the time-invariant eddy-viscosity models are those proposed by Grant and Madsen (1979) [henceforth GM79] and Christoffersen and Jonsson (1985) [henceforth CJ85]. They are based on a specific form for the eddy viscosity.

Although a modified version has been put forward by Madsen (1994), the CJ85 formulation is rather easy to handle through analytical solutions, facilitating its implementation in numerical models. Another model that does not consider the wave–current-interaction processes but is used routinely in wave spectral models to calculate the loss of energy by bottom friction is the JONSWAP model (Hasselmann et al., 1973).

According to Davies and Lawrence (1995), the use of GM79 has an impact on the three-dimensional circulation of the Irish Sea. Using a coupled wave-tide-surge model, Choi et al. (2003) showed that bottom velocity and the effective bottom-drag coefficient caused by the combination of waves and currents were higher than uncoupled cases. Working with a three-dimensional wave–current-coupled modeling system, Xie et al. (2003) concluded that storm surge prediction improved significantly when wave-induced surface stress and wave-induced bottom stress were taken into account. Some attempts have been made to quantify the wave, tide, and surge interaction in the North Sea by means of numerical simulations. Such studies deal with the effect of tide and surge on waves. According to Tolman (1990), tides in the North Sea offer an unsteady and heterogeneous medium for the propagation of waves. Currents are strong enough to favor wave–current interactions. The utility of 2D hydrodynamic models to determine the circulation in platform seas is adequate because the circulation is essentially 2D. This is true for the southern North Sea. The hydrodynamic characteristics of the southern North Sea and the presence of sandy sediments in the region allow the formation of sand banks in the study area off the Belgian Coast.

The coupled system used in our work has been described by Ozer et al. (2000). It consists of two numerical models; a modified version of the third-generation spectral-wave model WAM Cycle 4 (Komen et al., 1994, henceforth WAMC4) adapted for its implementation in coastal waters (Monbaliu et al., 2000, henceforth WAM-PRO), and a tide-surge model (Van den Eynde et al., 1995, henceforth TS). This coupled system has been used by Osuna and Monbaliu (2004) to study the impact of the interaction between waves, tides, and surges without considering the coupling effect on the bottom-boundary layer.

We refer to coupling as the one-way transfer of information from the TS model to the WAM-PRO model. The CJ85 formulation has already been included in the WAM-PRO model but it has been suggested that this still requires some testing (Ozer et al., 2000).

Our main objective was to assess the wave–current-interaction effect on the computation of bottom-shear stresses in coastal areas. The assessment is done using model–model result comparisons. A previous performance of the model is evaluated using integrated wave characteristics (significant wave height and mean period) using measurements and model results at two stations off the Belgian coast.

A brief description of the models used (WAM-PRO, TS, and CJ85) in the coupled system is presented in Section 2. The numerical experiments made and the meteorological and oceanographic conditions during the period of simulation are described in Section 3. In Section 4 the comparison between numerical experiments and a discussion of the results are presented. The conclusions are given in Section 5.

2. The models TS, WAM-PRO, and CJ85

The system that controls the models and the transfer of information between them has been developed and disseminated in the framework of the MAST III PROMISE Project (Prandle, 2000).

2.1. The TS model

The TS model is a revised version of an existing operational model used to forecast storm surges in the North Sea. It was developed by the Management Unit of Mathematical Models of the North Sea [MUMM] (Van den Eynde et al., 1995). It is a conventional, vertically integrated, two-dimensional shallow-water equations model, where the variables are depth-averaged current velocity, and elevation of the free surface relative to the mean sea level. The model solves the governing equations in Polar or Cartesian coordinates, which allows its implementation over wide geographical areas. The details of the model have been described by Osuna and Monbaliu (2004).

2.2. The WAM-PRO model

The WAM-PRO is a phase-average wave model, therefore it only delivers information about the energy density (or action density) for a discrete number of frequencies (or wave numbers) traveling in a discrete number of directions (the relative phase of these components is unknown). The evolution of the wave spectrum is described by the spectral-energy-balance equation (Komen et al., 1994). The governing equation includes advection in geographic and spectral (direction and frequency) space, refraction caused by depth and current (steady depth and current field only), the source terms associated with the wind input, the dissipation caused by white-capping, and the transfer of energy among components caused by nonlinear interactions. For the evaluation of the energy decay in shallow water, different bottom-friction formulations were added to the code. It can be set up for any local or global grid. The standard WAMC4 formulations for the source terms were used in this work, except for bottom-friction dissipation, where the CJ85 formulation was used (JONSWAP is the standard formulation to calculate bottom-friction dissipation in the WAMC4 model).

The source term for wave-energy dissipation because of bottom friction is

$$S_{\mathrm{bf}}(\omega,\theta) = -\frac{C_f}{g}\frac{\omega^2}{\sinh^2 \mathrm{kh}}F(\omega,\theta). \tag{1}$$

where C_f is a dissipation coefficient, g is the gravity acceleration, $F(\omega,\theta)$ is the energy-density spectrum in frequency-direction space, k is the modulus of the wave number vector $\mathbf{k}$, ω is the relative frequency, θ is the direction of $\mathbf{k}$ and h is the water depth.

According to Padilla-Hernández and Monbaliu (2001) the different formulations for the bottom friction dissipation differ mainly in the expression given to the dissipation coefficient C_f. For JONSWAP model it is assumed to be constant and given by

$$C_f = \frac{\Gamma}{g} \tag{2}$$

where Γ=0.038 m^2 s^{-3}.

2.3. The CJ85 formulation

The CJ85 model describes the velocity field and its associated bottom-shear stress in a combined wave–current motion by means of two two-layer eddy-viscosity models (Model I and Model II). The two models comprise the so-called current bottom-boundary layer (CBBL) and the wave bottom-boundary layer (WBBL). Models I and II have the same eddy viscosity in the CBBL, although they differ in the WBBL. Model I is valid for small values of $u_{*fm}/(k_b\omega_a)$ ($\leq$3.47) ("large roughness"), where u_{*fm} is the maximum friction velocity, ω_a is the absolute angular frequency and k_b is the bottom roughness length. Model II deals with large values of $u_{*fm}/(k_b\omega_a)$ ($\geq$3.47) ("small roughness"). A brief description is presented in Appendix A and the reader is referred to CJ85 for further details for Models I and II. The current is assumed steady and the bed locally horizontal. Lateral shear stresses in vertical sections, the Coriolis force and tidal forces are neglected. The current and wave friction factors (f_c and f_w) are defined as a function of depth-averaged current speed U, the amplitude of the wave-shear stress τ_{wbm} and the horizontal-wave orbital velocity (periodic component) at the bottom u_{wbm}. The maximum (total) bed shear-stress τ_{bm} is found to be

$$\tau_{bm} = \tau_{wbm}m = \frac{1}{2}mf_w\rho_w u_{wbm}^2 \tag{3}$$

where

$$m \equiv \sqrt{1+\sigma^2+2\sigma|\cos(\delta-\alpha)|} \tag{4}$$

and

$$\sigma \equiv \frac{\tau_{\mathrm{cb}}}{\tau_{\mathrm{wbm}}} = \frac{f_c}{f_w}\left(\frac{U}{u_{\mathrm{wbm}}}\right)^2 \tag{5}$$

Here α and δ are wave and current directions and σ is the ratio between the current (τ_{cb}) and the wave shear-stress.

The current friction-factor f_c is defined as for pure current motion (in the absence of waves), while the wave friction-factor f_w is thus defined for pure wave motion (in the absence of currents). In a combined wave–current motion, f_c and f_w become dependent on each other. The interactions between waves and currents are taken into account through the parameter m, which indicates the strength of the interactions. For pure wave motion m=1, and in the presence of currents m>1.

3. The numerical experiments

The coupled system was used for the North Sea region through a series of (four level) successively

Table 1
Types, geographic coverage, resolution, and time step (wave advection and source terms) for the various grids used in this work

Grid	Area	Res. (lat × lon)	Advection	Source
Coarse	47°50′N–71°10′N, 12°15′W–12°15′E	1/3° × 1/2°	WAM: 10 min, TS: 1 min	10 min
Local1	48°30′N–55°30′N, 02°45′W–09°15′E	1/15° × 1/10°	WAM: 2 min, TS: 1 min	10 min
Local2	49°14′N–52°38′N, 00°03′E–04°45′E	1/45° × 1/30°	WAM: 1 min, TS: 1 min	10 min
Fine	50°59′N–51°30′N, 02°27′E–03°53′E	1/135° × 1/90°	WAM: 30 s, TS: 15 s	5 min

Bathymetry fields used are the same as those included in the coupled system from Osuna and Monbaliu (2004).

nested grids (Coarse, Local2, Local1, and Fine grids). The geographic coverage for each of the grids used and the most relevant grid characteristics are given in Table 1. The set up is similar to the one used by Osuna and Monbaliu (2004).

During the nesting procedure, the boundary conditions for the (relatively finer) inner grids were generated by the correspondent relatively coarser grid runs from the uncoupled system. For the wave model, the JONSWAP formulation for bottom-friction dissipation was used. The outputs from the finest grid are the results we used for the intercomparisons made in this study. For the TS model, the nesting process consisted of the transfer of the elevation of free surface (η) values stored from a coarser grid at points matching the open boundary points of the finer grid. The η values of the rest of the finer grid boundary points are then interpolated with a polynomial method. The data were stored at every coarse time-step and used for the nested grid with no time interpolation.

Hydrodynamic variables and the wave field were recorded at the two stations Westhinder (WHI) at 51°23′04″N and 02°26′40″E at 13.2 m depth and Bol Van Heist (BVH) at 51°22′45″N and 03°12′29″E at 11.9 m depth. A detailed bathymetry of the finest grid and the location of the stations are shown in Fig. 1.

Meteorological data (horizontal components of wind velocity at 10 m and atmospheric pressure) to force the models were provided by MUMM and the United Kingdom Meteorological Office (UKMO). Wind data were supplied at 6-hour intervals on a 1.25° latitude–

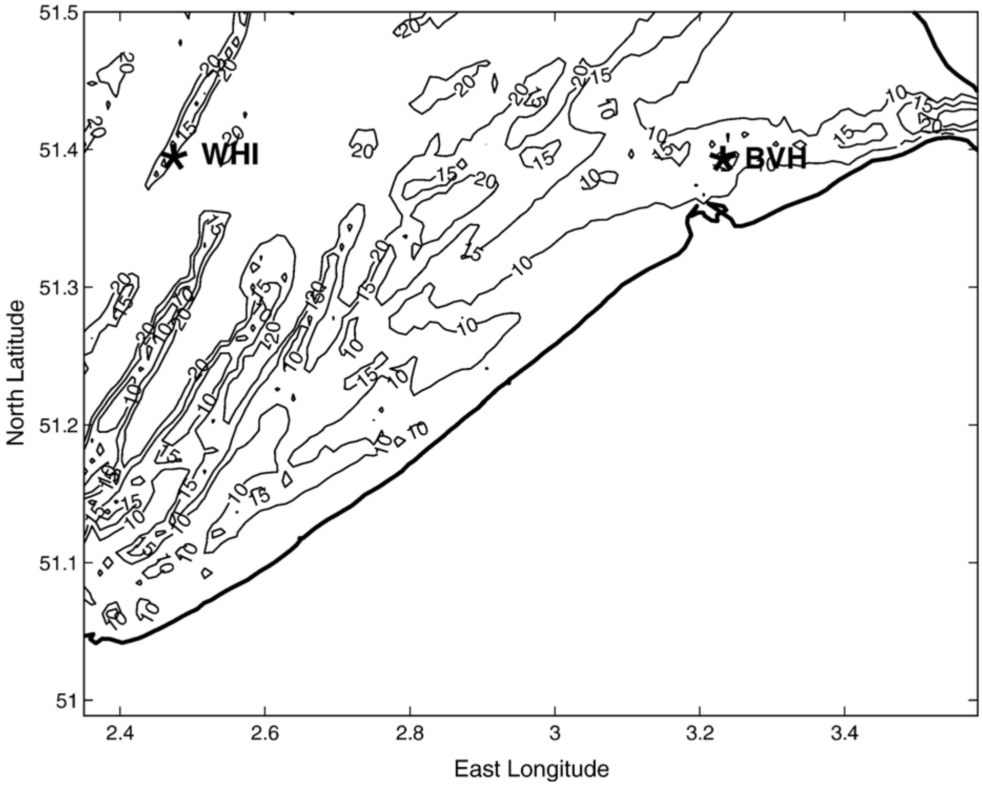

Fig. 1. Bathymetry of the fine grid and location for stations Westhinder (WHI) and Bol Van Heinst (BVH). Depths are in meters.

longitude resolution grid at 0000 GMT and 1200 GMT from analysis and at 0600 GMT and 1800 GMT from forecasting. Model results from 5 to 20 October 1997 were analyzed. During our study period, two events are highlighted and referred to for detailed analysis, which events were characterized by rather strong winds (speeds up to 15 m/s) and different directions. Event 1) was between days 7 and 11, southwesterly winds increasing from 5 m/s to 15 m/s were dominant and event 2) following a rapid shift in wind direction, a sustained northwesterly wind during days 12 to 16 with speeds between 10 m/s and 15 m/s was measured. Wind characteristics for the simulation period collected at WHI station are shown in Fig. 2.

Four numerical experiments were made. The Experiments I and III were made with no transfer of information between the TS and WAM-PRO models (uncoupled runs). The JONSWAP formulation for bottom-friction dissipation calculation was used in Experiment I (reference run) and the CJ85 formulation was used in Experiment III. The experiments II and IV were made with the transfer of information from the TS model to the WAM-PRO (one-way coupling). The transferred information was the elevation of the free surface (η) and the current field (u, v). The formulations used to calculate the bottom-friction dissipation were the JONSWAP for experiment II and CJ85 for experiment IV (see Table 2).

To use the CJ85 formulation, it is necessary to define a value for the roughness-length parameter (k_b). According to Luo and Monbaliu (1994), when using the flow condition in the southern North Sea a typical value is $k_b = 0.02$ m. Because the shear stress calculated by the model system, when using the CJ85 formulation, is in the form of a stress matrix (as a function of frequency and direction), convenient integral parameters were defined to allow comparisons of results when the JONSWAP formulation was used (the JONSWAP formulation provides a single value at each grid point and time-step).

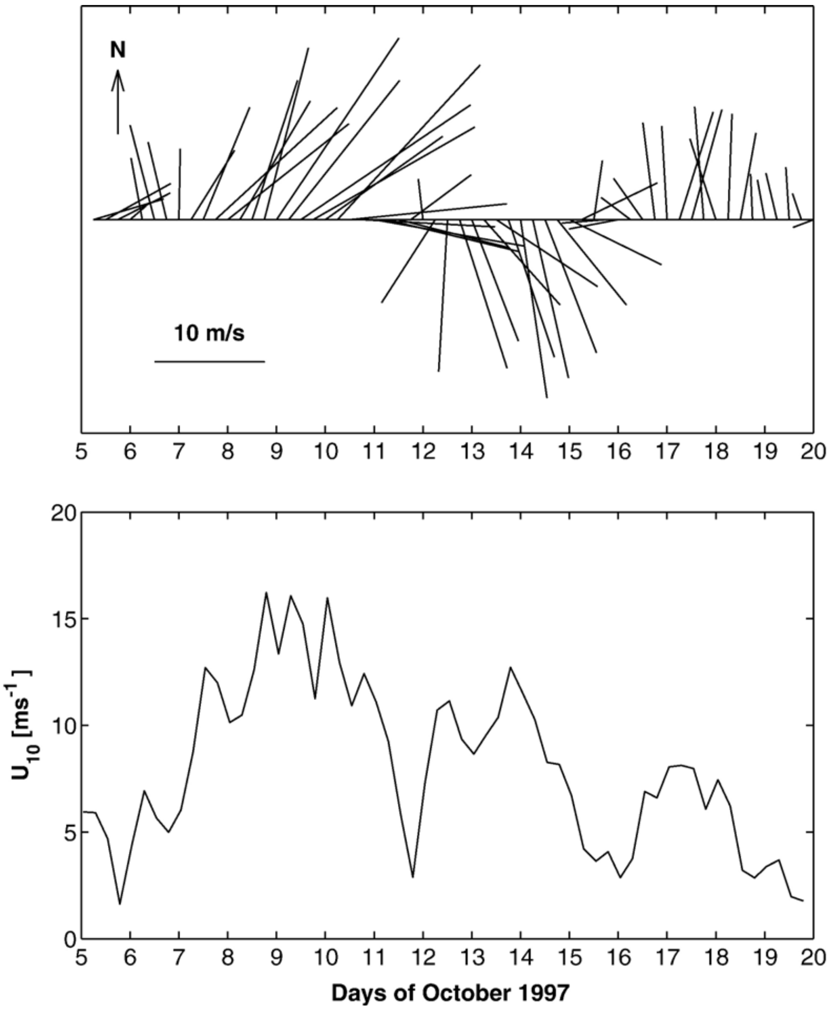

Fig. 2. Wind conditions during the period of simulation. Wind data from the U. K. Met. Office and extracted from data base for WHI station location (51°23′04″N 02°26′40″E).

Table 2
Details and reference code of the numerical experiments made

Experiment code	Description	Bottom friction coefficient formulation
I	Uncoupled	JONSWAP (reference)
II	Coupled	JONSWAP
III	Uncoupled	CJ85
IV	Coupled	CJ85

Uncoupled system refers to experimental runs with no exchange of information between the wave model WAM-PRO and the hydrodynamic (currents) model TS. Coupled system refers to experimental runs where TS model transfers η, u and v to WAM-PRO.

The shear stress associated with the spectral peak-wave component in this work was equal to the maximum shear stress ($\tau_{\max}$). The mean shear stress ($\overline{\tau}$) was calculated by

$$\overline{\tau} = \int_0^\infty \int_0^{2\pi} \tau(\sigma,\theta) w(\sigma,\theta) d\sigma d\theta \tag{6}$$

where

$$w(\sigma,\theta) = \frac{\tau(\sigma,\theta)}{\int_0^\infty \int_0^{2\pi} \tau(\sigma,\theta) d\sigma d\theta} \tag{7}$$

4. Results

The comparisons between the numerical-experiment results are presented in this section. A brief description of the numerical experiment and reference codes are given in Table 2. Because the main objective of this work was to determine the effect of including the wave–current-interaction process on the bottom stress, no attempt was made to calibrate the models to reproduce the observed fields more precisely.

4.1. Experiments I and II

The time-series of measurements and model results (Experiments I and II) are shown in Fig. 3 for the WHI and BVH stations. Two events with moderate to high waves can be observed. During the first event (from 7 to 11 October), the significant wave height (H_s) was up to 3.2 m and during the second (from 12 to 15 October) H_s was 3.8 m maximum. These two events are associated with different wind regimes, a southwesterly wind for the first period and a northwesterly wind for the second.

Both experiments underestimate H_s, although the differences between the measured and model results are smaller for low-wave conditions. According to Monbaliu et al. (1997), Cardone and Resio (1998), and Ozer et al. (2000), the WAMC4 (the basis for WAM-PRO) model tends to underestimate H_s and T_{m02}, especially during stormy periods. In Fig. 3 it is evident from the H_s time-series that underestimation decreases toward the coast. At WHI the bias for H_s (see definition in Appendix A) is −0.23 m and −0.21 m for Experiments I and II, whereas at BVH the bias is −0.12 m and −0.11 m for Experiments I and II. The time-series of T_{m02} show a similar trend of underestimation, mainly observed during stormy events, which tends to decrease toward the coast (bias = −0.27 s at WHI and −0.07 s at BVH for Experiment II). Cardone and Resio (1998) suggested that the propagation scheme implemented in the WAMC4 model would produce an underestimation of swell energy. For the conditions of the Belgian coast, this would lead to a relatively more pronounced underestimation of H_s and T_{m02} during northerly winds, because there will be a longer propagation time to reach station BVH than for the southerly winds, which show a better agreement for observed and simulated H_s fields. It is also evident from Fig. 3 that a better qualitative agreement between measured T_{m02} and Experiment II is found, in particular for oscillations associated with the tidal influence (including similar phase).

The time-series of the difference of H_s (ΔH_s) and T_{m02} (ΔT_{m02}) (Experiment II minus Experiment I) are shown in Fig. 4. The impact of coupling is clear, with ΔH_s and ΔT_{m02} of the order of ±0.18 m and ±1.0 s. During stormy periods H_s differences increase at station WHI, especially during southwesterly winds. At station BVH (shallower region), increased differences in H_s are easily observed during storm events when high waves are present. It is readily apparent from both time-series (ΔH_s and ΔT_{m02}) that oscillations are associated with the variation of sea level caused by semidiurnal tides (Osuna and Monbaliu, 2004).

According to linear-wave theory, variations in T_{m02} depend on current velocity and the intrinsic frequency of the wave field. During Experiment II (coupled system), variations of sea level (η) and the velocity field (u and v) were transferred from the TS model to the WAM-PRO model, which explains the variations shown in Fig. 4.

The bottom-shear stress estimated from Experiments I and II at stations WHI and BVH are shown in Fig. 5 (panels a and c). The maximum values for shear stress are of the order of ±3 N/m^2. The effect of coupling the TS and WAM-PRO models is observed as slight variations all during the simulation period, whereas the oscillations associated with tidal variations are rather more apparent, even during periods of relatively low waves (15 to 19 October).

The bottom-shear-stress difference between Experiments I and II was of the order of ±0.4 N/m2, at the most (Fig. 5, b and d). Larger differences are associated

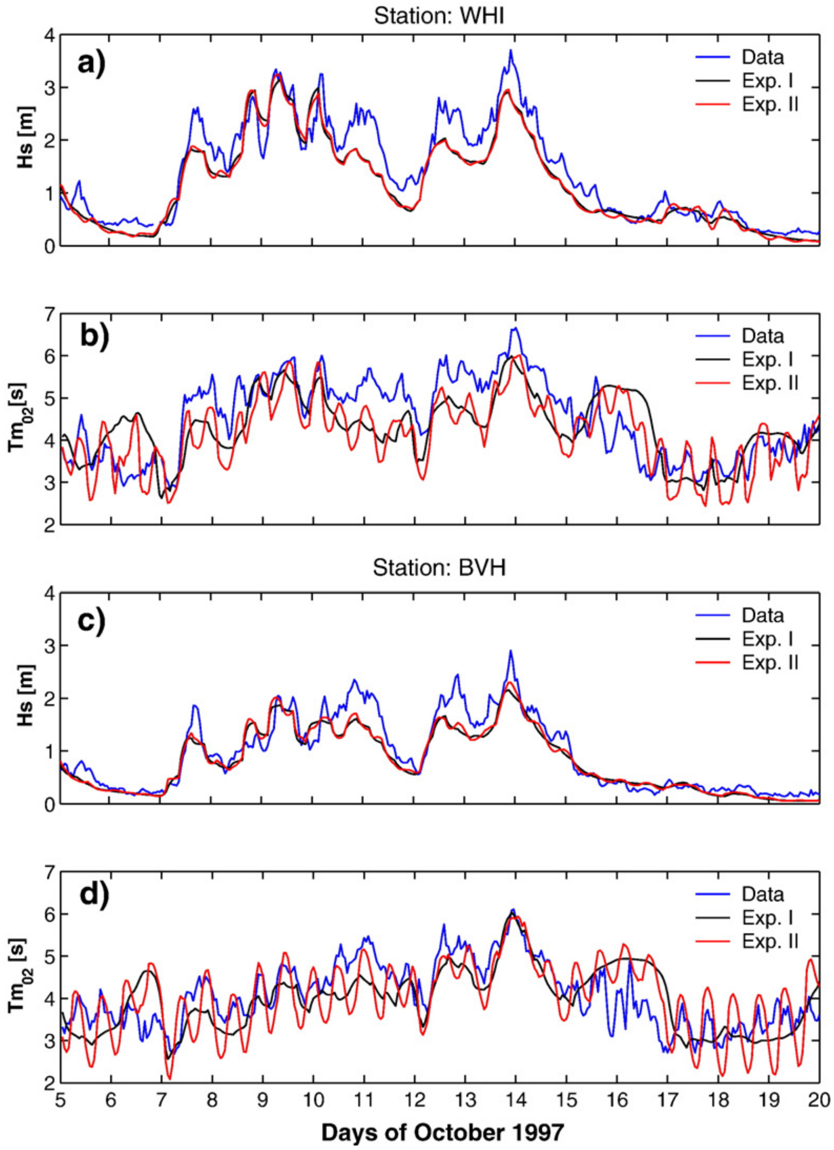

Fig. 3. Time-series for a) H_s and b) T_{m02} at station WHI and for station BVH (c and d) from measurements (blue line), and from Experiment I (black line) and Experiment II (red line).

with higher waves during storm periods (7 to 11 and 12 to 15 October), especially at station WHI where the significant wave height is higher than that at station BVH.

4.2. Experiments I and III

To look in detail into the effect of the two different formulations to calculate the dissipation coefficient (C_f) on the bottom-friction-source function (S_{bf}) and on the bottom-shear stress (τ), a comparison is made between results from Experiments I and III. Both experiments were made as uncoupled systems (no information about η, u or v was transferred from the TS model to the WAM-PRO model).

Because the two experiments (I and III) are uncoupled, no effect from tidal oscillations are expected nor observed in wave parameters.

The bottom-shear stress (τ) time-series calculated from Experiments I and III (mean and maximum) at stations WHI and BVH are shown in Fig. 6. At station WHI (Experiment III) τ_{max} was generally greater than that calculated from Experiment I, whereas at station BVH this was not true. Differences in τ_{max} between Experiments I and III at WHI are greater during southwesterly winds (7 to 11 October) compared to northwesterly winds (13 to 15 October). During periods of low waves (5 to 8 and 16 to 20 October) the bottom-shear stress values were similar in both experiments.

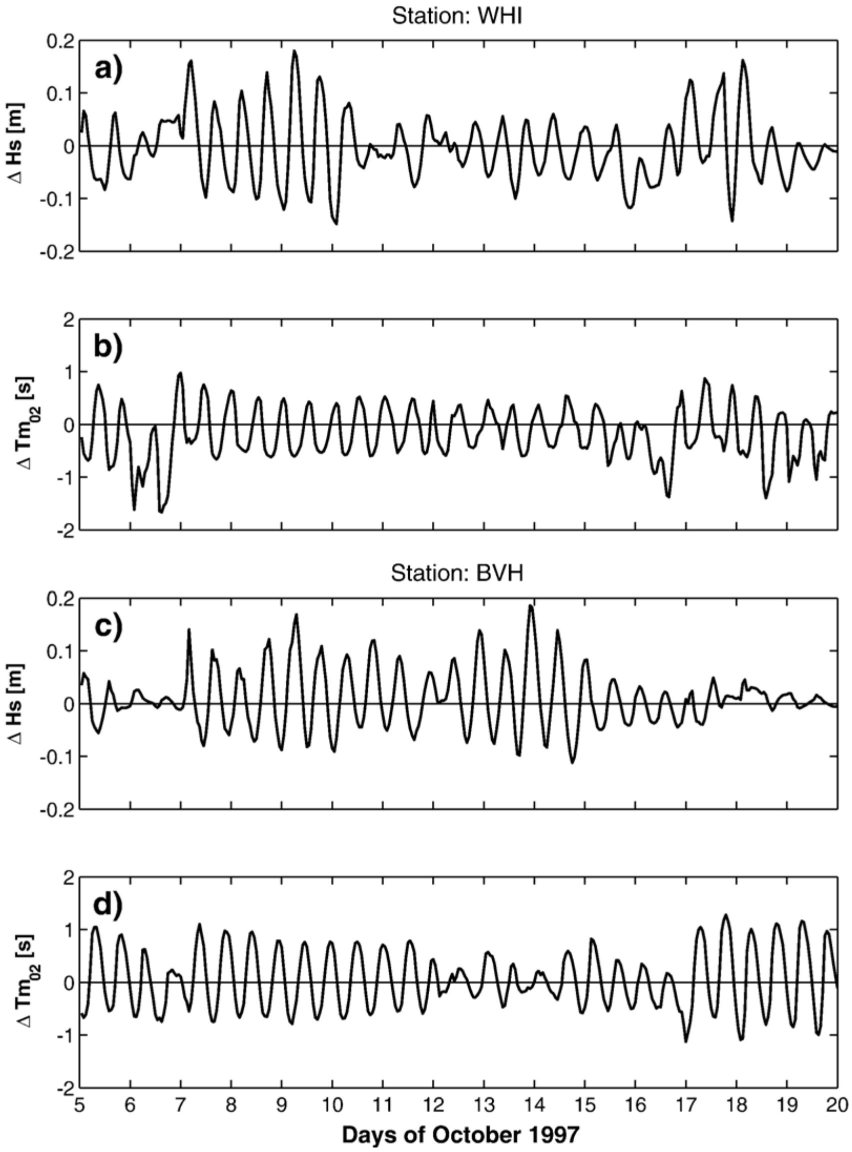

Fig. 4. Time-series for differences of Hs and T_{m02} from Experiment I relative to experiment II (Exp. II–Exp. I) at stations WHI (a and b) and BVH (c and d).

Even during conditions of relatively high waves (9 to 12 October, for instance) at station BVH (shallow region), the bottom-shear stress determined from Experiment I was greater than τ_{max} from Experiment III.

During southwesterly winds (9 to 12 October) τ_{max} is greater at station WHI than that simulated at station BVH and is caused by higher waves generated from the larger fetch associated with station WHI. For the northwesterly winds however, the active fetch would be similar for both stations. However, waves were higher at station WHI than those at station BVH because the latter station is shallower and the bottom effect causing energy dissipation is larger.

The mean shear stress ($\overline{\tau}$) from Experiment III is always lower than the bottom-shear stress estimated from Experiment I. This represents some evidence for uncertainty in using the mean value ($\overline{\tau}$) for sediment-transport estimations for instance.

Focusing on the spatial distribution of the bottom-shear stress, the difference of the results between Experiment III (τ_{max}) and Experiment I (τ) was determined ($\Delta\tau = \tau_{max} - \tau$). Three specific times associated with the presence of large waves for each of the southwesterly and northwesterly wind events were selected; 9 October at 0900, 1200, and 1800 (southwesterly winds) and 13 October at 1500, 1800, and 2100 (northwesterly winds). The corresponding evolution of the wave field during these periods obtained from Experiment IV is shown in Fig. 7. The significant wave height is color-coded and the arrows represent the mean wave direction. The wind is considered uniform for the whole Fine grid, wind

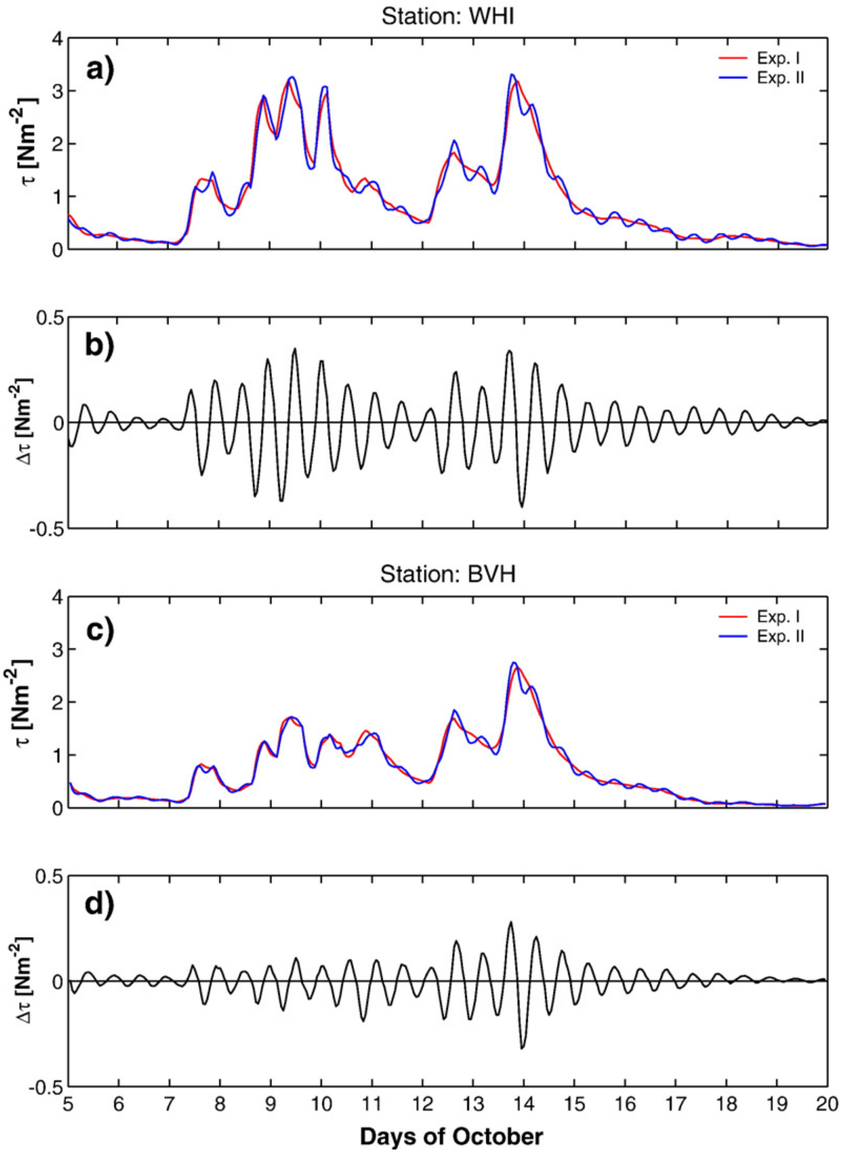

Fig. 5. Time-series for τ at a) station WHI and c) station BVH from Experiment I (red line) and Experiment II (blue line). Bottom-shear-stress differences between Experiments II and Experiment I for b) station WHI and d) station BVH.

speed is given in m/s, and the blue arrow shows the wind direction. The evolution for the bottom-shear-stress difference fields ($\Delta\tau$) is shown as a sequence in Fig. 8, for the same dates and times as for the previous figure (left panels for 9 October and right panels for 13 October). Positive values show regions where τ_{max} (Experiment III) was greater than τ computed from Experiment I.

For southwesterly winds (left panels in Fig. 8), positive values are generally observed away from the coast for the three selected times whereas negative values are measured near the coast. The effect of sand bars is readily apparent for these results where positive values are shown in the western portion of the area of interest. Positive values cover less area in the last time frame at 1800 when decreasing wave height is observed, showing only a slight influence of the more prominent sand bars, still in the southwestern portion.

Right panels in Fig. 8 represent ($\Delta\tau$) results from northwesterly wind conditions (13 October at 1500, 1800, and 2100). Wave-height fields showed (Fig. 7) higher energy from the first (1500) to the last (2100) time frames. As wave height increased, the bottom-shear stress from Experiment III also increased showing wider areas in panels with positive values for ($\Delta\tau$), especially for the upper half portion. It becomes apparent that the sand banks in the northeastern portion of the area do influence the bottom-shear stress, especially when high waves approach from the north.

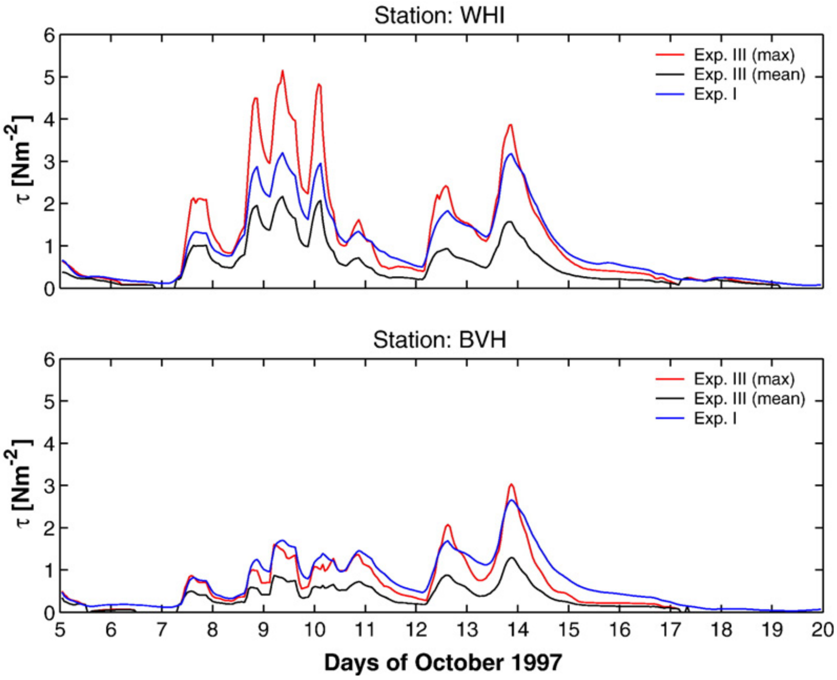

Fig. 6. Time-series of τ_{max} (red line), $\overline{\tau}$ (black line), and τ (blue line) from Experiment III and Experiment I at stations WHI (upper panel) and BVH (lower panel), during October 1997.

4.3. Experiments I and IV

A comparison is made between results from Experiment IV and the reference experiment (Experiment I). In a plot showing the difference between H_s obtained from Experiment IV and that obtained from Experiment I (not shown), small oscillations associated with sea level variations are observed, caused by the transfer of η information from TS to WAM-PRO. The effect of coupling in experiment IV is also observed in the T_{m02} time-series for both stations. Oscillations related to the effect of the semidiurnal-tide component through the Doppler shift are noticeable.

In Experiment IV, the bottom-shear stress is calculated by taking into account the wave–current interactions. Important differences become readily apparent when compared to results from those experiments where no consideration of this interaction is given.

In Fig. 9 the maximum bottom-shear stress (τ_{max}) and mean bottom-shear stress ($\overline{\tau}$) obtained from Experiment IV are shown as along with the bottom-shear stress (τ) from Experiment I at stations BVH and WHI. For low-wave conditions (5 to 7 and 15 to 17 October), the maximum and mean bottom-shear stresses are similar, including the presence of oscillations caused by variations in currents and sea level. Larger differences are observed during storm periods.

In particular, at station WHI values for τ from Experiment I (blue line in Fig. 9) are almost always lower than τ_{max} obtained from Experiment IV, especially during storm periods (7 to 11 and 13 to 15 October).

During low wave conditions at the BVH station, the bottom-shear stress obtained from Experiment IV (both mean and maximum) shows a strong influence of the tidal effect, where maximum values are as high as those in high-wave conditions. For instance, the maximum values obtained from Experiment IV during the first part of the simulation period (5 to 7 October) are of the order of 3 Nm^{-2} whereas the bottom-shear stress from Experiment I is only about 0.2 Nm^{-2}. A similar influence from tidal conditions is observed for other low-wave periods (15 to 17 October).

The bottom-shear-stress values at station BVH are lower than those at station WHI during storm periods. During low-wave conditions the situation is reversed with higher values for the bottom-shear stress measured at station BVH. It is generally observed that waves are lower at the shallower station BVH then at WHI. Furthermore, primary and secondary maxima for bottom-shear stress are alternatively obtained during low-wave conditions at station BVH, though not at station WHI.

To compare the bottom-shear stress obtained from experiment IV (τ_{max}) to the reference run (τ calculated from Experiment I), the difference field ($\Delta\tau$) is determined and shown color-coded in Fig. 10, along with the current field obtained from the TS model (black arrows). The tidal elevation and phase are given in the inset of each panel for reference. In a similar fashion as in Fig. 8,

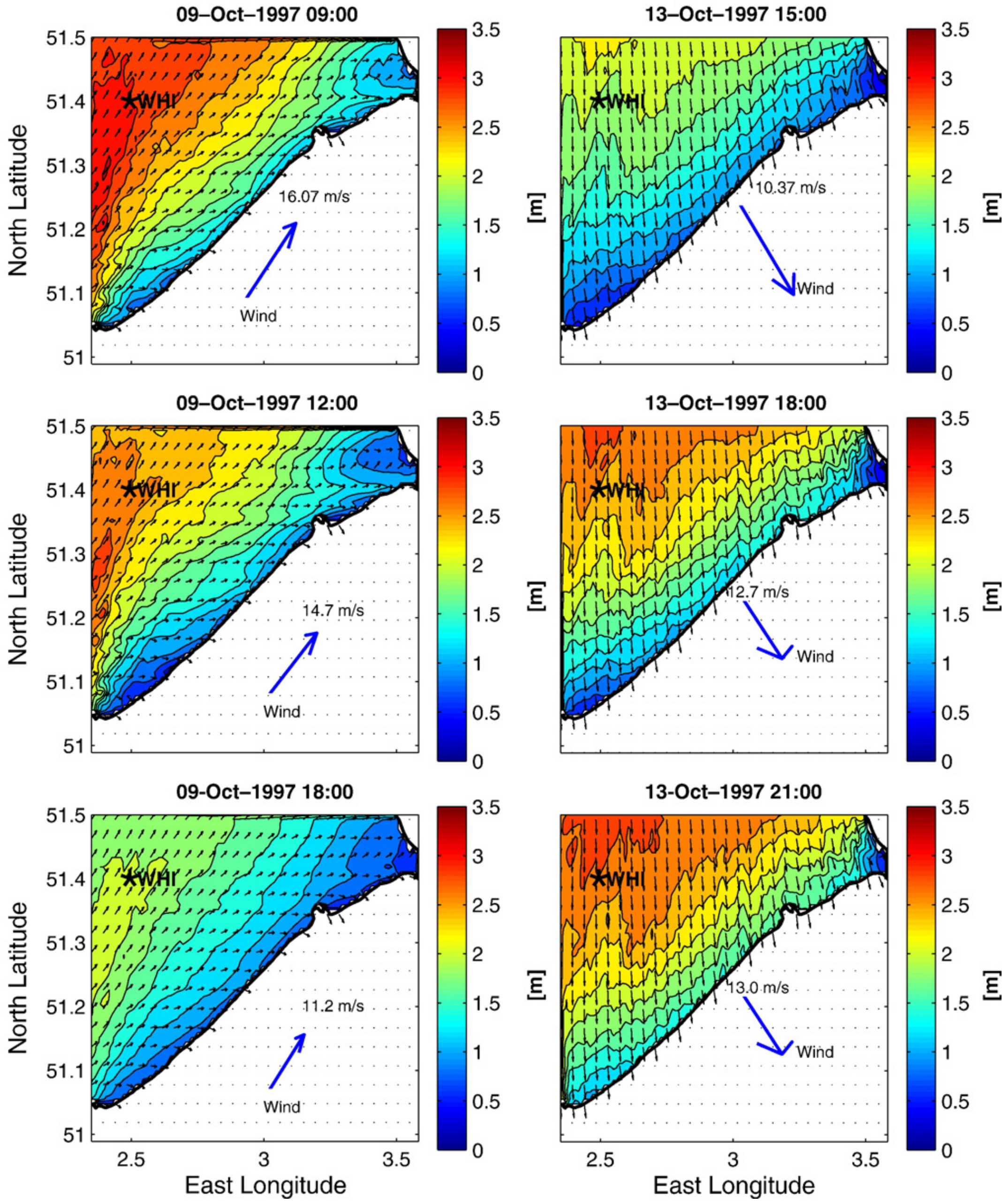

Fig. 7. Wave-height fields (H_s color coded and given in meters) and mean wave direction (black arrows) for the study area and representative wind conditions (m/s) taken at WHI station (blue arrows) for typical southwesterly (left panels) and north-westerly winds (right panels). Times selected for southwesterly winds are 0900, 1200, and 1800 on 9 October and for northwesterly wind conditions are 1500, 1800, and 2100 on 13 October.

$\Delta\tau$ is shown for southwesterly winds in the left panels and for northwesterly winds in the right panels. The spatial distribution of $\Delta\tau$ is given for the specific times already selected (Fig. 8) for uncoupled run comparisons. Reference for significant wave height and mean wave-direction fields can also be obtained from Fig. 7 (results from Experiment IV).

From 9 October at 0900 to 1200 the significant wave height was decreasing though the mean wave direction remained similar. Near low water and low tide the current speed changed considerably (from moderate to slow). At 1800, although the significant wave height was still decreasing (that was the lowest of the three times shown here), the current field intensified with a northeast direction. Important changes in the bottom-shear-stress fields are readily apparent from the current-field influence, as shown in Fig. 10 (bottom left panel). Whereas the areas with positive values for $\Delta\tau$ are only depicted around sand banks and submerged sand bars for the first two times shown (0900 and 1200), results for (τ_{max}) in experiment IV were higher than those from the reference run (τ calculated from Experiment I) at 1800

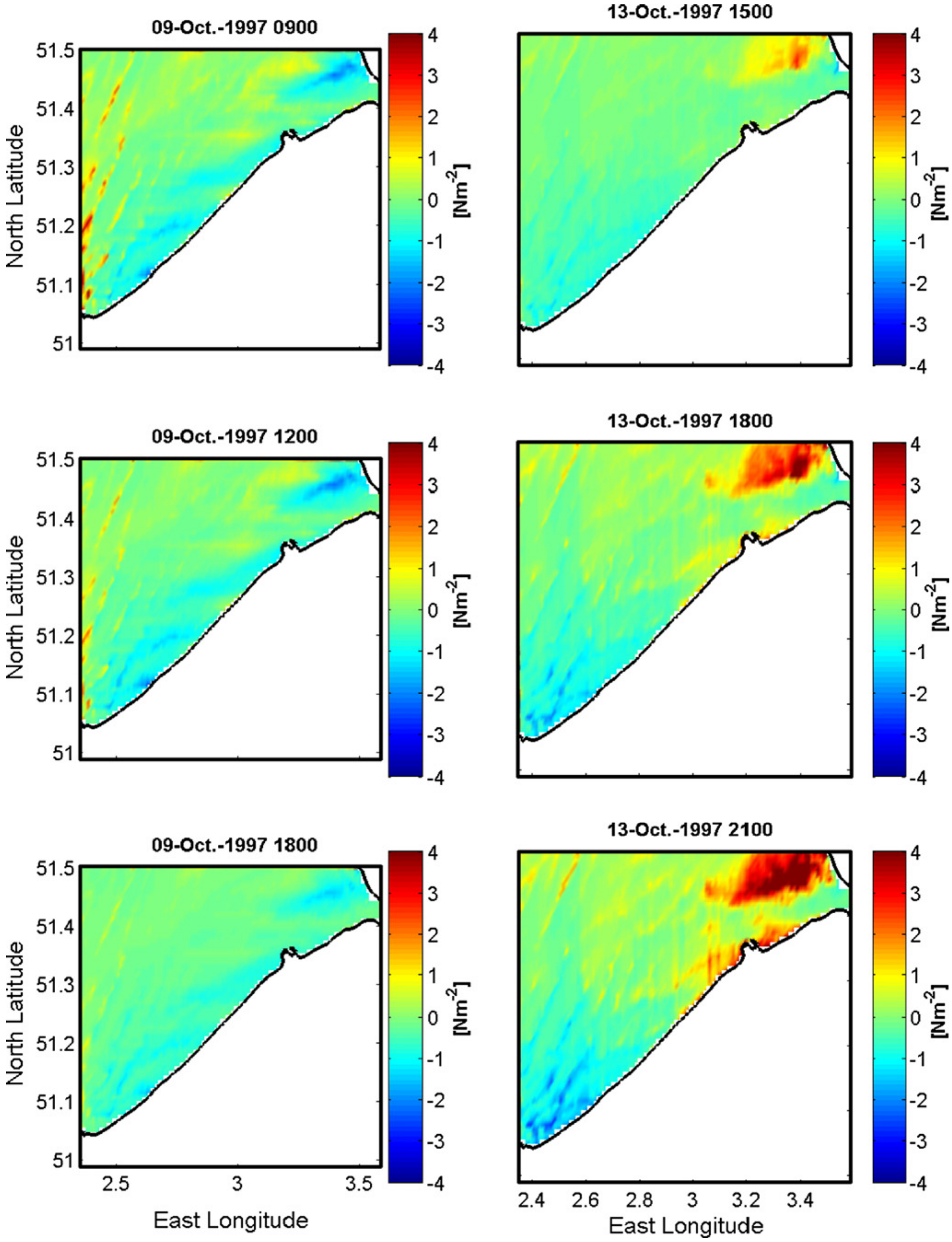

Fig. 8. Bottom-shear-stress differences ($\Delta\tau$) between Experiment III and Experiment I for typical southwesterly (left panels) and northwesterly wind conditions (right panels). Selected dates and times are the same as for Fig. 7.

for almost the whole study area. However, the effect of the underwater sand bars was barely observed.

Relatively high waves and low to moderate currents at low tide cause enhancement of τ_{max} compared to τ, particularly at sand banks and underwater sand bars. These features can be clearly identified from $\Delta\tau$ maps at 0900 and 1200.

For northwesterly winds, on 13 October, significant wave height increased from 1500 to 2100 (highest), whereas the current field was from weak to moderate also at 1500 and 2100 hours, and rather strong between those times.

Low waves and weak currents still cause a high $\Delta\tau$ around sand banks and underwater sand bars (13 October

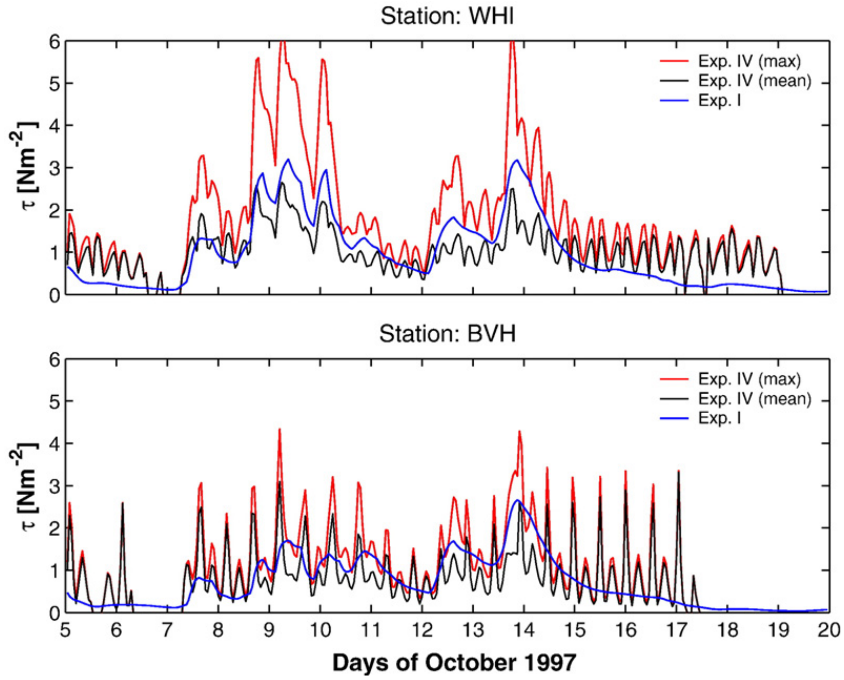

Fig. 9. Time series of $\tau_{\max}$ (red line), $\overline{\tau}$ (black line), and τ (blue line) for Experiment IV and Experiment I at stations WHI (upper panel) and BVH (lower panel) during October 1997.

at 1500) and are depicted as positive values. Stronger currents and higher waves will show as a positive $\Delta\tau$ almost over the whole study area (13 October at 1800), with the particular condition that the tidal elevation was low. In contrast (low currents), three hours later the underwater sand bars did not cause high values of $\Delta\tau$ even if this were the time of the highest waves of these three times because the water level was high. Furthermore, large positive values of $\Delta\tau$ were only observed at the sand bank regions and the upper part of the coastal area under study, where the waves first arrived as they approached from the north.

The combination of moderate to high waves and strong currents on 13 October at 1800 causes an important enhancement of $\tau_{\max}$ (calculated from Experiment IV) compared to the bottom-shear stress from the reference run (Experiment I). Low tidal elevation is expected to increase the wave effect at the bottom compared to the next time when even higher waves did not show significantly high positive values for $\Delta\tau$, mainly because of the higher tide.

4.4. Experiments III and IV

In this section, results from Experiment III (uncoupled runs) are compared to those from Experiment IV (coupled runs). Both experiments used the CJ85 formulation to compute the loss of energy by bottom friction. The difference between the time-series (not shown) of H_s at stations WHI are of the order 0.05 m and at station BVH are of the order 0.15 m. The effect of coupling is rather more pronounced for H_s at the BVH station. Oscillations caused by the semidiurnal tide are evident from the T_{m02} time-series at both stations. The maximum shear stress ($\tau_{\max}$) computed from Experiments III and IV at both stations (WHI and BVH) are shown in Fig. 11. In general the shear stress computed during Experiment IV was greater than that calculated in Experiment III. Differences are greater at the BVH station, even in low-wave conditions (days 5 to 7 and 15 to 17). It is apparent that during these periods, shear stress is controlled mainly by the tidal current. During stormy periods shear stress is mainly caused by wave orbital-velocities, as can be deduced, because differences between shear stress computed by Experiments III and IV are small and do not show oscillations caused by the tide (days 8 to 11 at station WHI). During decreasing wave height at station WHI the shear stress differences are more pronounced (days 5 to 7 and 15 to 17), thus it is clear that shear stress is strongly influenced by tidal oscillation.

Fig. 11 shows that at station WHI bottom-shear stress differences are larger during a northwesterly wind; at BVH the opposite occurs. This is caused by the distribution of wave heights predicted by the uncoupled and coupled systems.

The bottom-shear stress difference fields ($\Delta\tau$) between Experiments IV and III for three selected times on 9 and 13

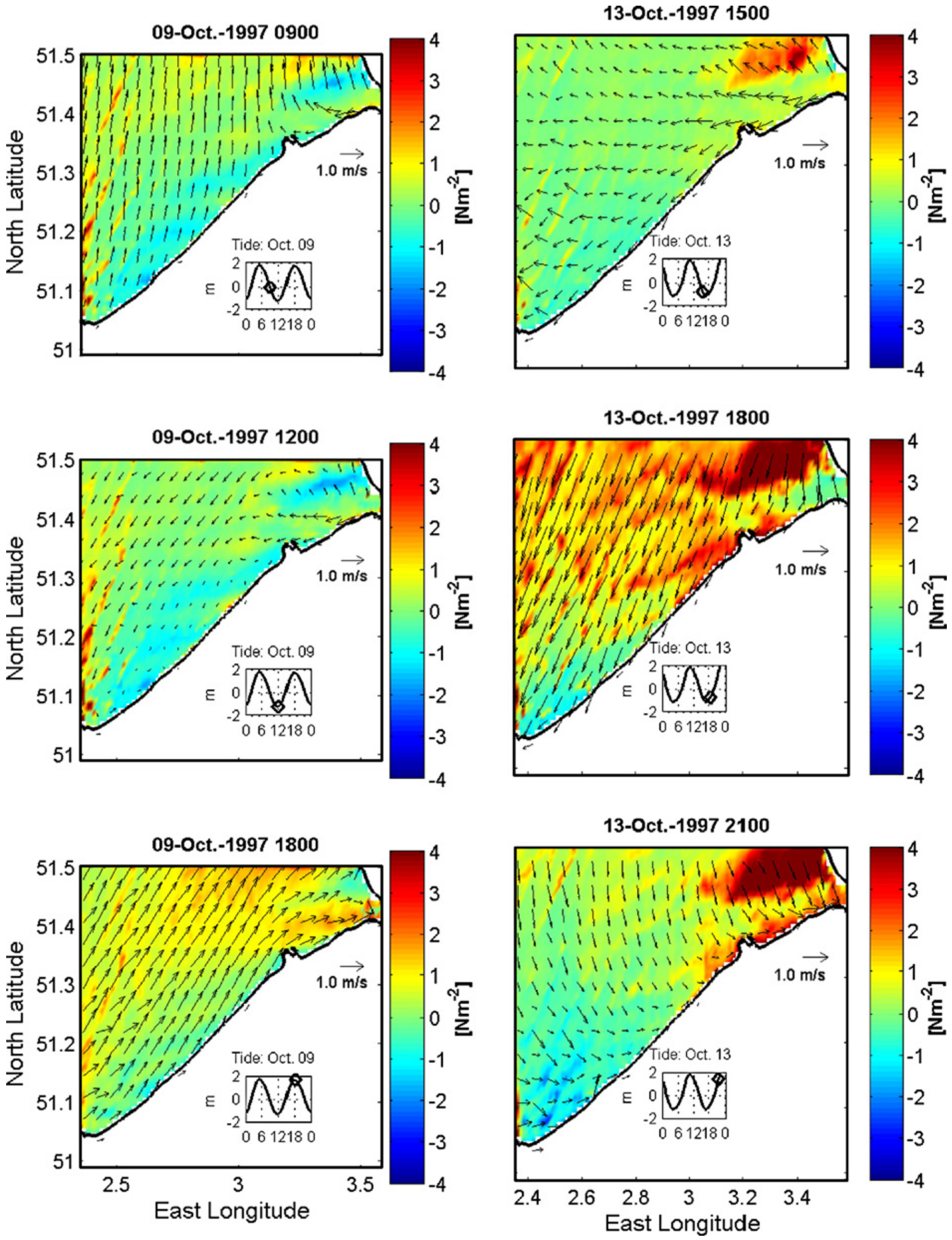

Fig. 10. Bottom-shear-stress differences ($\Delta\tau$) between Experiment IV and Experiment I for typical southwesterly (left panels) and northwesterly wind (right panels). Selected dates and times are the same as for Fig. 7.

October are shown in Fig. 12. Tides and currents are also included (left panels for southwesterly winds and right panels for northwesterly winds).

We recall that the wave height decreased whereas the mean wave direction remained rather constant on 9 October from 0900 to 1800 (southwesterly wind) as shown in Fig. 7. There it can be seen that the wind speed gradually decreased. The difference field for bottom-shear stress between Experiments IV and III at 0900 is rather small, nearly zero for most of the study area (see top left panel in Fig. 12).

There are slightly positive $\Delta\tau$ values over the sand banks (northeast portion of the study area) associated with the current field effect (enhancing) on the estimation of bottom-shear stress for Experiment IV through the wave–current interaction.

At 1200 positive values for $\Delta\tau$ are more pronounced at the southwest underwater sand bars. The current field is in the opposite direction to the waves and some negative $\Delta\tau$ values are depicted over the sand banks (northeast portion of the study zone). Because of the low tide, this could lead us to suggest an important role of the

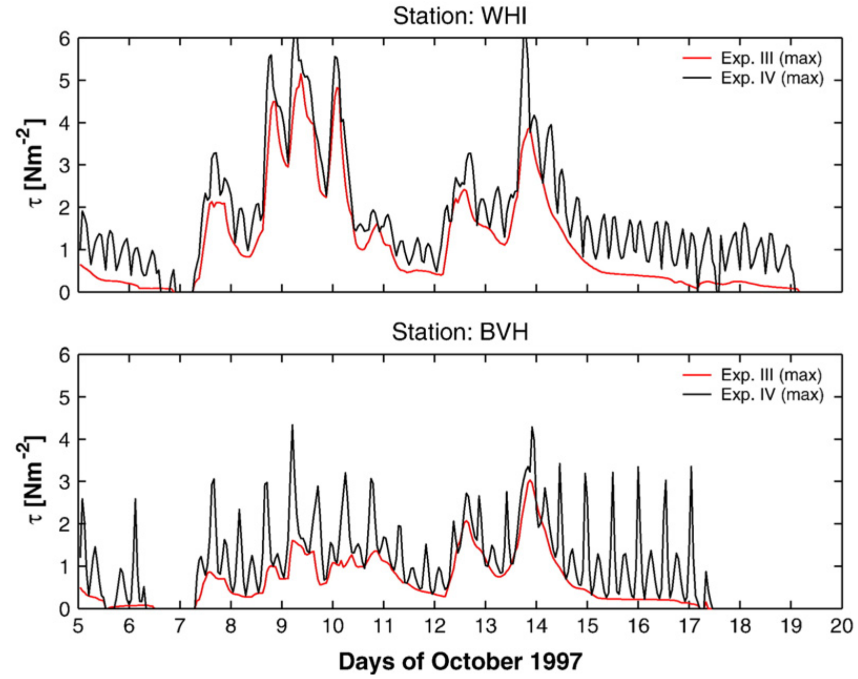

Fig. 11. Time-series of τ_{max} at stations WHI (upper panel) and BVH (lower panel) during October 1997 for Experiment III (red line) and Experiment IV (black line).

water depth on the intensification of bottom stress. At 1800 the current field is intense and positive $\Delta\tau$ values are more pronounced though the current field shows the same direction as the waves. Enhancement of wave–current interaction is expected, according to Eq. (3), because the m parameter (Eq. (4)) indicates the interaction strength depends on the relative direction between waves and currents. Even if the waves are relatively low (compared with conditions at 0900 and 1200), $\Delta\tau$ is generally larger.

The difference in the bottom-shear stress ($\Delta\tau$) for a northwesterly wind is shown in the right panels of Fig. 12. The wind speed increased from just over 10 m/s to 13 m/s from 1500 to 2100 on 13 October. Wave height also increased during that time.

The greatest bottom-shear stress from Experiment IV is obtained when moderate to high waves and strong currents are moving in the same direction (13 October at 1800), not only over the sand banks (northeastern portion of the study area) and the underwater sand bars (southwestern region), but also almost over the whole area of interest where positive $\Delta\tau$ values are observed. Earlier (at 1500), the current direction was perpendicular to the wave direction of propagation and some positive $\Delta\tau$ values were measured mainly over the sand bank and underwater sand bars, where the strongest currents are. At 2100 the water level is high and the current speed rather moderate in almost the same direction of the waves. Nevertheless, the bottom-stress differences $\Delta\tau$ were close to zero except over the sand banks.

5. Conclusions

An evaluation of the effect of considering wave–current interaction on the bottom-shear stress calculations has been made through numerical modeling using a system with the capability of coupling waves and currents. The coupled system included a tide surge model (TS) transferring information of the sea surface elevation and currents to a wave model (WAM-PRO).

Four numerical experiments were run and their results were compared. Two of the experiments used the uncoupled version of the system (with no exchange of information between the models) with different formulations to calculate the dissipation coefficient in the expression to compute the wave energy dissipation caused by bottom friction. One of the formulations used (CJ85) does consider the interactions between waves and currents.

The effect of coupling the hydrodynamic and the wave models is clearly observed in the time series for H_s and T_{m02}, even for the simplest cases when the JONSWAP formulation was used to calculate the bottom-friction dissipation as in Experiments I and II. Oscillations in H_s, T_{m02}, and τ results can easily be associated with tidal influence. Furthermore, the time-series of the difference of H_s and τ show greater differences between Experiments

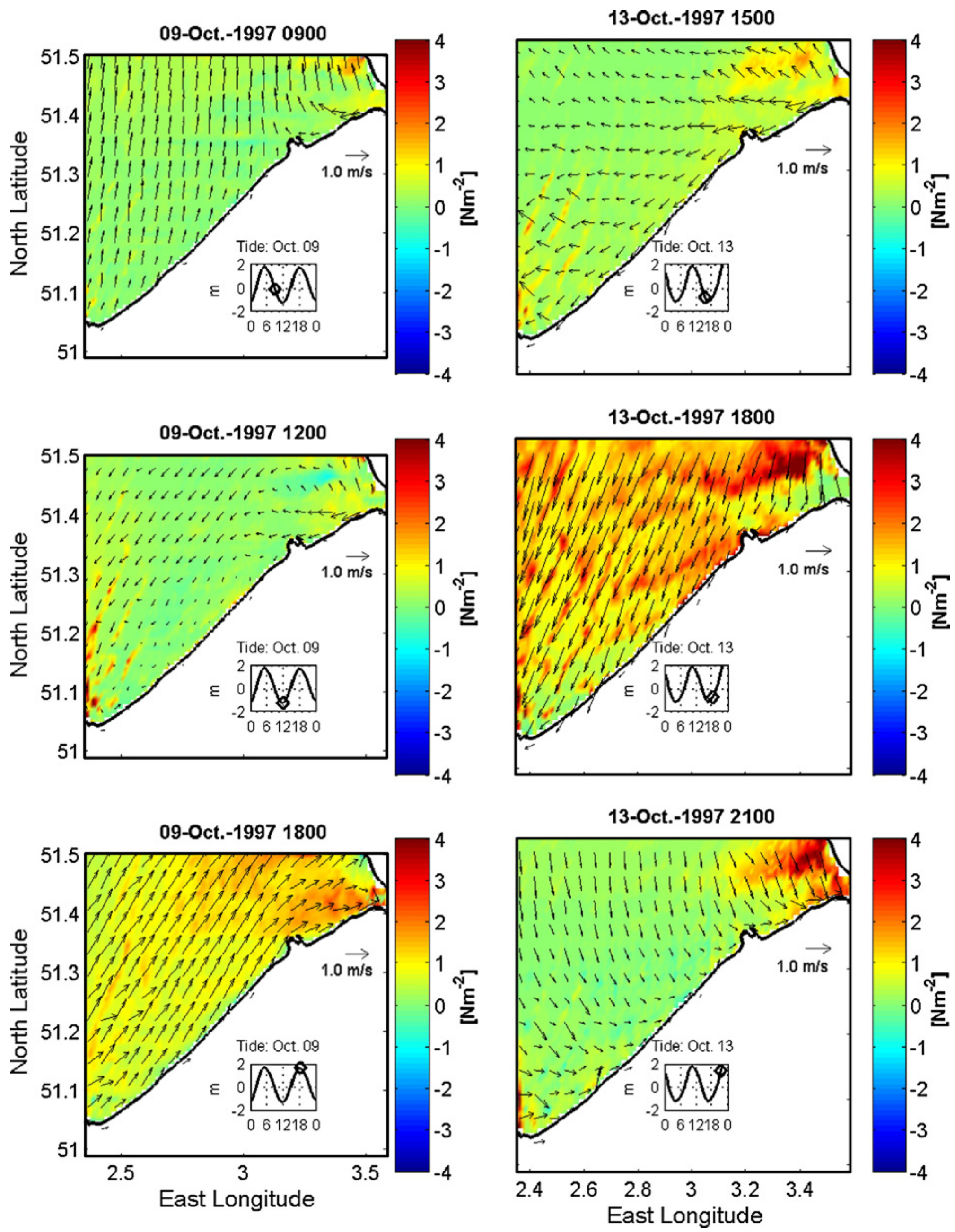

Fig. 12. Bottom-shear-stress differences ($\Delta\tau$) between Experiment IV and Experiment III for typical southwesterly (left panels) and northwesterly winds conditions (right panels). Selected dates and times are the same as for Fig. 7.

II and I for the high-wave periods, although the tidal influence was detected over the whole simulation period. When the coupling system was used the only influence from the current field was through advection in the wave model, whereas the bottom-dissipation calculation was affected by the depth variations caused by tidal elevation. The bottom-shear-stress difference between Experiments I and II was of the order of 0.5 Nm^{-2} at most. Larger differences were associated with higher waves during storm periods (7 to 11 and 12 to 5 October), especially at station WHI for the significant wave heights are slightly higher than those at station BVH.

When the uncoupled system was used (Experiments I and III), differences between model results were more pronounced at the shallower station BVH, mainly caused by the energy dissipation and bottom friction. The bottom-shear stress calculated by the CJ85 formulation showed in general greater values than the results using JONSWAP scheme. For southwesterly winds, the bottom-shear-stress enhancement was observed using CJ85 over the underwater sand bar area, whereas for northwesterly winds a similar enhancement was observed over the shallow areas at the northeast portion of the simulated area. The results clearly show that the formulation of the bottom-friction dissipation that accounts for the effect of wave–current interaction has a significant effect on the determination of the bottom-shear stress.

When using the CJ85 formulation, enhanced bottom-shear stress was obtained if the coupled system was used (comparing the results from Experiments III and IV), particularly when the current field showed the same direction as the waves (See middle right panel in Fig. 12). The enhancement was only moderate over the sand banks and underwater sand bars for other current field directions. It is therefore evident that the wave height plays a partial role on the bottom-shear-stress estimations. A similar enhancement over the whole area was also found for moderate to low waves under southwesterly wind conditions (See bottom left panel in Fig. 12).

Acknowledgements

P. Rosales would like to acknowledge the scholarship provided by the National Council for Science and Technology (CONACyT, México) and Instituto Tecnológico de Guaymas. This is a contribution of project SEP-2003-C02-44718 supported by CONACYT. The authors also received some support for research stays under the Mexico-Belgium agreement between CONACYT and FNRS (J200.760/2003). Thanks to Dr. Ellis Glazier for editing of the English-language text.

Appendix A. Mean absolute error (mae) or bias definition and a brief description of the CJ85 model

$$\text{mae} = \left[\sum(\mathbf{m}-\mathbf{o})\right]/N = \overline{\mathrm{m}} - \overline{\mathrm{o}} \tag{A.1}$$

where $\overline{\mathrm{o}}$ and $\overline{\mathrm{m}}$ represent the mean values of the observations (**o**) and predictions (**m**). $\sum$ indicates summation over the elements of the vector in question.

A1 CJ85 model (brief description)

The equation describing horizontal equilibrium in the CJ85 model is

$$\frac{\partial \mathbf{u}}{\partial t} + (\mathbf{u}\cdot\nabla)\mathbf{u} + w\frac{\partial \mathbf{u}}{\partial z} + \frac{1}{\rho_w}\nabla p = \frac{\partial}{\partial z}\left(\frac{\tau}{\rho_w}\right) \tag{A.2}$$

Here **u** is the total horizontal particle velocity, t is time, z is the vertical Cartesian coordinate measured upwards from the bed, w is the vertical particle-wave velocity, $\nabla(=\partial/\partial x, \partial/\partial y)$ is the horizontal gradient operator, x and y are horizontal Cartesian coordinates, ρ_w is the water density, p is the total pressure, and τ is the total shear stress in a horizontal section. The quantity p and the horizontal velocity u consist of a steady (current) part and oscillating (wave) part, i.e.

$$p = p_c + p_w \; ; \; \mathbf{u} = \mathbf{u}_c + \mathbf{u}_w \tag{A.3}$$

The **subscripts** c and w indicate the components caused by the current and the wave. Using the eddy viscosity concept, the shear stress is expressed as the vector sum of wave and current stress

$$\tau = \tau_c + \tau_w \; ; \tau_b = \tau_{\mathrm{cb}} + \tau_{\mathrm{wb}} \tag{A.4}$$

where the **subscript** b indicates a quantity at the bed.

From the Eq. (A.2) the governing equations for the current and wave motion are derived. For the current motion the equation is

$$\rho_w \epsilon_c \frac{\partial \mathbf{u}_c}{\partial z} = \tau_c(1 - z/h) \tag{A.5}$$

where ϵ_c is the eddy viscosity in the current-boundary layer and h is the water depth. For the wave motion within the wave-boundary layer the governing equation is

$$\frac{\partial}{\partial t}(\mathbf{u}_w - \mathbf{u}_{\mathrm{wb}}) = \frac{\partial}{\partial z}\left(\frac{\tau_w}{\rho_w}\right) = \frac{\partial}{\partial z}\left(\epsilon_w \frac{\partial \mathbf{u}_w}{\partial z}\right) \tag{A.6}$$

where ϵ_w is the eddy viscosity and $\mathbf{u}_{wb}$ is the horizontal-wave orbital-velocity at the top of the wave-boundary layer.

The solutions of the Eqs. (A.5), (A.6) provided expressions for the current (f_c) and wave (f_w) friction factors for combined current-wave motion, these are determined from

$$\sqrt{\frac{2}{f_c}} = \frac{1}{\kappa}\ln\frac{30h}{ek_N} + \frac{1}{\kappa}\ln\frac{k_A}{k_b} \tag{A.7}$$

where κ is the von Kármán constant (=0.40) and k_A is the apparent roughness, which is larger than the bottom roughness k_b because of the effect of the waves.

$$\frac{m}{4.07\sqrt{mf_w}} + \log\frac{1}{4.07\sqrt{mf_w}} = -0.1164 + \log\left(\frac{a_{\mathrm{bm}}\omega_r}{k_b\omega_a}\right) \tag{A.8}$$

where m is the ratio of the total bed-shear stress to the wave component of the shear stress, a_{bm} is the wave orbital semiexcursion, ω_a is the absolute wave angular-frequency, and ω_r is the relative wave angular-frequency. Wave and current friction factors are iteratively solved to convergence, then the maximum bed stress is given by

$$\tau_{bm} = \frac{1}{2} f_w \rho_w u_{\mathrm{wbm}}^2 m \tag{A.9}$$

where u_{wbm} is the periodic component of the horizontal velocity at the bottom.

References

Cardone, V.J., Resio, D.T., 1998. An assessment of wave modelling technology. Proceedings of the 5th International Workshop on Wave Hindcasting and Forecasting, Melbourne, Florida. Atmospheric Environment Services, Ontario, pp. 468–495.

Choi, B.H., Eum, H.M., Woo, S.B., 2003. A synchronously coupled tide-wave-surge model of Yellow Sea. Coast. Eng. 47, 381–398.

Christoffersen, J.B., Jonsson, I.G., 1985. Bed friction and dissipation in a combined current and wave motion. Ocean Eng. 12 (5), 387–423.

Davies, A.M., Lawrence, J., 1995. Modeling the effect of wave–current interaction on the three-dimensional wind-driven circulation of the Eastern Irish Sea. J. Phys. Oceanogr. 25 (1), 29–45.

Grant, W.D., Madsen, O.S., 1979. Combined wave and current interaction with a rough bottom. J. Geophys. Res. 84 (C4), 1797–1808.

Hasselmann, K., Barnett, T.P., Buows, E., Carlson, H., Cartwright, D.E., Enke, K., Ewing, J.A., Gienapp, H., Hasselmann, D.E., Kruseman, P., Meerburg, A., Muller, P., Olbers, D.J., Richter, K., Sell, W., Walden, H., 1973. Measurements of wind-wave growth and swell decay during the Joint North Sea Wave Project (JONSWAP). Dtsch Hydrogr. Z. 8 (12), 95 (Suppl. A).

Jonsson, I.G., 1990. Wave–current interactions. In: LeMehaute, B., Hanes, D.M. (Eds.), The Sea, Ocean Engineering Science, vol. 9A. J. Wiley and Sons, New York, pp. 65–120.

Komen, G.J., Cavaleri, L., Donelan, M., Hasselmann, S., Hasselmann, K., Janssen, P.A.E.M., 1994. Dynamics and modelling of ocean waves. Cambridge University Press, Cambridge. 532 pp.

Luo, W., Monbaliu, J., 1994. Effects of the bottom friction formulation on the energy balance for gravity waves in shallow water. J. Geophys. Res. 99 (C9), 18,501–18,511.

Madsen, O.S., 1994. Spectral wave–current bottom boundary layer flow. Proc. 24th Int. Conf on Coastal Eng. Coastal Eng. Res. Council, ASCE, Kobe, pp. 384–398.

Malarkey, J., Davies, A.G., 1998. Modelling wave–current interactions in rough turbulent bottom boundary layers. Ocean Eng. 25 (2-3), 119–141.

Monbaliu, J., Zhang, M.Y., De Becker, K., Hargreaves, J., Luo, W., Flather, R., Carretero, J.C., Gomez-Lahoz, M., Lozano, I., Stawarz, M., Günther, H., Rosenthal, W., Ozer, J., 1997. WAM model intercomparisons—North Sea. Report, vol. 47. Proudman Oceanographic Laboratory, Birkenhead.

Monbaliu, J., Padilla-Hernández, R., Hargreaves, J.C., Carretero-Albiach, J.C., Luo, W., Sclavo, M., Günther, H., 2000. The spectral wave model WAM adapted for applications with high spatial resolution. Coast. Eng. 41, 41–62.

Osuna, P., Monbaliu, J., 2004. Wave–current interaction in the Southern North Sea. J. Mar. Syst. 52, 65–87.

Ozer, J., Padilla-Hernández, R., Monbaliu, J., Alvarez Fanjul, E., Carretero Albiach, J.C., Osuna, P., Yu, J.C.S., Wolf, J., 2000. A coupling module for tides, surges and waves. Coast. Eng. 41, 95–124.

Padilla-Hernández, R., Monbaliu, J., 2001. Energy balance of wind waves as a function of the bottom friction formulation. Coast. Eng. 43, 131–148.

Prandle, D., 2000. Operational oceanography in coastal waters. Coast. Eng. 41, 3–12.

Tolman, H.L., 1990. Wind wave propagation in tidal seas. Commun. Hydraul. Geotech. Eng. Delft University of Technology, The Netherlands.

Van den Eynde, D., Scory, S., Malisse, J.-P., 1995. Operational modelling of tides and waves in the North Sea on the Convex C230 at MUMM. European Convex User's Conference 1995, 24-27 October 1995, Brussels, Belgium.

Xie, L., Pietrafesa, L.J., Wu, K., 2003. A numerical study of wave–current interaction through surface and bottom stresses: coastal ocean response of Hurricane Fran of 1996. J. Geophys. Res. 108 (C2), 3049. doi:10.1029/2001JC001078.